Scientia Iranica, Vol. 10, No. 2, pp 142–152

SCIENTIA
IRANICA

Boundary Element Method Applied to the Cavitating Hydrofoil and Marine Propeller

H. Ghassemi[1]

A Boundary Element Method (BEM) for the calculation of hydrodynamic characteristics and flow analysis, including cavitation, is presented. The effectiveness of the method is demonstrated with results for a partially cavitating, three-dimensional hydrofoil and a marine propeller. The method employs source and dipole singularities, which give an integral equation on body and cavity surfaces, to obtain the cavity shape and hydrodynamic characteristics of the cavitating hydrofoils. A nonlinear formula of the dynamic boundary condition was applied for determining the potential on the cavity surface. The effect of the cross-flow was considered when calculating the velocity on the cavity surface. The lift and drag coefficients, pressure distribution and cavity shape of the hydrofoil were calculated and compared with experimental results for a cavitating hydrofoil. The calculated results show good agreement with the experimental values. Flow velocity fields around the cavitating hydrofoils were also investigated by the present method. The method was extended to a marine propeller (with cavitation) and, again, good comparisons were found. However, further improvement can be made if the definition of the cavity separation and cavity trailing edge is improved, in order to achieve exact cavity area.

INTRODUCTION

One of the main objectives of the present research was to find the hydrodynamic characteristics and flow field analysis around cavitating hydrofoils and marine propellers. Cavitation may occur anywhere in a liquid where the velocity increases and the pressure diminishes below the vapor pressure. Designers of marine systems often try to avoid cavitation because of its detrimental effect on hydrofoil boats, marine propellers, pumps and turbines. Cavitation can be useful in other areas, such as medical, physical and biological applications.

Modern research in computational hydrodynamics is linked to the development of the computer and many numerical methods were developed during the second half of the twentieth century. Among computational tools was the BEM, which is a powerful tool for the analysis of configuration problems, with good accuracy and low computational time. As a result, many researchers have applied this method and, as a result, it has become optimized for particular problems. The first three-dimensional application for cavitation was in 1980, for the modeling of the flow around a propeller with the lifting surface method [1]. Kinnas and Fine [2,3] used the potential based BEM applied to 2- and 3-dimensional partially cavitating hydrofoils with a closed type model of the sheet cavity. They found a pressure discontinuity at the cavity trailing edge with a closed type model. Ando et al. [4] used SQCM (simplified surface panel method) for a three-dimensional steady cavitating hydrofoil. The author [5] also employed the potential-based panel method to two- and three-dimensional cavitating hydrofoils by using a closed type model at the cavity trailing edge.

The problem of a cavity trailing edge is, actually, more complicated and difficult. As cavitation is a viscous effect, using Navier-Stokes equations should be more suitable for bubble and cloud cavitation, which is unsteady, has a two phase flow and is highly turbulent. Kubota et al. [6] developed a two phase flow model by solving the Navier-Stockes equations, using the Findition-Difference Method (FDM) on the two-dimentional flow field around a hydrofile.

In the present method, following the Kinnas and Fine method, an open type of cavity model has been used. An open type model is assumed at the cavity trailing edge, to recover pressure distribution through an iterative method to obtain the cavity shape, with a specified gap at the cavity trailing edge. This may be addressed by some assumption regarding the cavity

1. *Department of Marine Technology, Amirkabir University of Technology, Tehran, I.R. Iran.*

model, in order to recover pressure distribution on the cavity.

Using Green's third identify, the perturbation velocity potential at any point in the flow field can be written by an integral equation, in terms of source and dipole singularities. The dynamic boundary condition on the cavity surface should be applied, simultaneously, with Green's formula to obtain the exact nonlinear solution of potential flow on the body and cavity surfaces. However, the usual problem to be faced is that the position of the cavity surface is unknown. As a first iteration towards the fully nonlinear solution, one may assume the initial cavity length and calculate the potential and source strength on the cavity and body (non-cavity) surfaces. At each iterative process, the body and cavity surfaces are re-paneled, based on the updated cavity shape, which was computed at the end of the previous iteration.

Lift and drag coefficients are calculated at different angles of attack for an NACA0012 elliptic hydrofoil, where the cavitation number is changed from a non-cavitating condition to a partially cavitating condition. The results obtained by this method are compared with experimental results and the capability of the method is demonstrated. The flow field around the cavitating hydrofoil is also calculated using this method and presented in this paper.

The method was extended to predict the cavity shape and hydrodynamic characteristics of a marine propeller. Experimental data for a propeller, including cavitation, are very scarce. Propeller model SRI-123 was found here to be compared with the present computational results. The calculated hydrodynamic characteristics in a cavitating condition are presented and compared with available experimental data.

The remainder of the paper is organized as follows. First, the mathematical formulation and boundary conditions are described. Then, the numerical results are presented and compared with experimental data for both the cavitating hydrofoil and the marine propeller. Finally, conclusions and recommendations are provided.

MATHEMATICAL FORMULATION

Basic Equation and Boundary Conditions

In order to proceed with BEM, the total velocity potential, Φ, and the perturbation velocity potential, ϕ, are related as follows:

$$\Phi = \vec{V}_I.\vec{x} + \phi, \tag{1}$$

where $\vec{V}_I$ and $\vec{x}$ are the inflow velocity and the position vector, respectively.

Restricting this study to the case where the perturbation flow is inviscid (high Reynolds number), irrotational and incompressible, the flow field around a body is represented by a perturbation velocity potential, ϕ, which satisfies the Laplace equation:

$$\nabla^2\phi = 0. \tag{2}$$

A boundary value problem can be constructed by specifying boundary conditions on the surfaces of the cavity and body, as follows:

i) The Kinematic Boundary Condition (KBC) is that the velocity, normal to the body and cavity surfaces, S_B, should be zero.

$$\nabla\Phi.\vec{n} = 0, \quad \text{on } S_B U S_C. \tag{3}$$

ii) There is no flow or velocity jump across the wake surface, while the potential jump is allowed across the wake and equal to the circulation, Γ, around the body. It is expressed in the perturbation potential as:

$$\triangle\left(\frac{\partial\phi}{\partial n}\right)_{S_W} = \left(\frac{\partial\phi}{\partial n}\right)^U - \left(\frac{\partial\phi}{\partial n}\right)^L = 0, \tag{4}$$

$$(\triangle\phi)_{S_W} = \phi^U - \phi^L = \Gamma, \tag{5}$$

where indexes U and L mean upper and lower sides of the body, respectively:

iii) The Kutta condition at the Trailing Edge (TE) states that the flow velocity at the TE remains bounded, i.e.:

$$|\nabla\phi|_{TE} < \infty. \tag{6}$$

iv) The Dynamic Boundary Condition (DBC) on the cavity surface, i.e. the pressure on the cavity surface, will be constant for the steady cavity flow and equal to the cavity (vapor) pressure p_c.

$$p = p_c. \tag{7}$$

The cavity surface is not known in advance and, hence, an approximate cavity shape is, initially, assumed, where the singularities are to be positioned. For this approximate shape, the tangential flow boundary condition (Equation 3) will not be satisfied. The problem is, therefore, to displace the approximate surface in such a way that the requirement (Equation 3) may be met through iterations.

Given the pressure distribution from DBC (Equation 7), the interacted tangential velocity, V_T, is determined by assuming the existence of a cross-flow velocity component, which is perpendicular to the chordwise flow component and which will effect the total velocity potential, especially at the tip of the

hydrofoil or propeller blade. Therefore, it is important, in three-dimensional problems, to take the deviation of velocity in the spanwise direction into account.

Considering a non-perpendicular coordinate system, as shown in Figure 1, S and ν denote chordwise and spanwise directions, respectively. This coordinate system is at the cavity surface starting from the point, l_d. Then, chordwise and cross-flow velocities are computed, as follows:

$$V_s = \partial\Phi/\partial s, \tag{8}$$

$$V_r = \frac{\partial\Phi/\partial\nu - \partial\Phi/\partial s\cos\theta}{\sin\theta}, \tag{9}$$

where $\partial\Phi/\partial\nu$ and $\partial\Phi/\partial s$ are the spanwise and chordwise velocity, respectively, and θ is the angle between them.

The gradient of the potential on the cavity can be expressed as:

$$\nabla\Phi = V_s\vec{s} + V_r\vec{r}. \tag{10}$$

On the other hand, the absolute value of the gradient of total potential is the total tangential velocity, V_c:

$$|\nabla\Phi| = V_c. \tag{11}$$

From Equations 10 and 11, after substituting and simplification, the following solution for the interacted tangential velocity, V_T, on the cavity surface s_c is obtained as:

$$V_T = \cos\theta\frac{\partial\Phi}{\partial\nu} + \sin\theta\sqrt{V_c^2 - \left(\frac{\partial\Phi}{\partial\nu}\right)^2}, \tag{12}$$

where, V_c is a known operating condition, as follows:

$$V_c = V_I\sqrt{1+\sigma}, \tag{13}$$

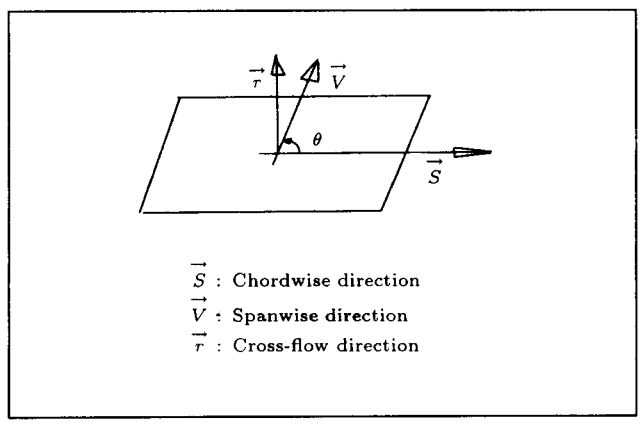

Figure 1. Local coordinate system on the panel. Vectors $\vec{S}$ and $\vec{\nu}$ are formed by lines connecting the midpoints of the lines connecting the panel vertices.

where σ is the cavitation number. The general formula for the cavitation number may be expressed as follows:

$$\sigma = \frac{p_\infty - p_c}{1/2\rho V_I^2}. \tag{14}$$

The cavitation number depends on the local inflow velocity for each element. Here, it can be expressed for propeller and hydrofoil as follows:

$$V_I = V_0 \quad \text{for hydrofoil,}$$

$$V_I = \left(V_A^2 + (2\pi rn)^2\right)^{1/2} \quad \text{for propeller.} \tag{15}$$

Knowing the velocity on the cavity surface, one can, then, compute the total potential on the cavity surface, s_c, as follows:

$$\Phi(s_c) = \int_{l_d}^{s_c} V_T ds_c. \tag{16}$$

Discretization of Equation 16 affords the following equation:

$$\Phi(s_c) = \sum_{n=1}^{N_c} V_T\triangle s_c + \Phi(l_d). \tag{17}$$

$\Phi(l_d)$ is the total potential on the cavity starting point and it is known from the 'without cavity' condition. One may consider that the cavity starts from the leading edge, $l_d = 0$. Then, the perturbation potential is calculated from $\phi(s_c) = \Phi(s_c) - \vec{V}_I\vec{x}_c$. The coordinate system and schematic of the open type model of the cavity on a hydrofoil is shown in Figure 2.

A boundary panel formulation is obtained by applying Green's theorem to solve Laplace's equation:

$$4\pi\phi(p) = \int_{S_B}\left\{\phi(q)\frac{\partial}{\partial n_q}\left(\frac{1}{R(p;q)}\right) - \frac{\partial\phi(q)}{\partial n_q}\left(\frac{1}{R(p;q)}\right)\right\}dS + \int_{S_W}\triangle\phi(q)\frac{\partial}{\partial n_q}\left(\frac{1}{R(p;q)}\right)dS, \tag{18}$$

where $R(p;q)$ is the distance from the field point, p, to the boundary point, q. This equation may be regarded as a representation of the velocity potential, in terms of a normal dipole distribution of strength,

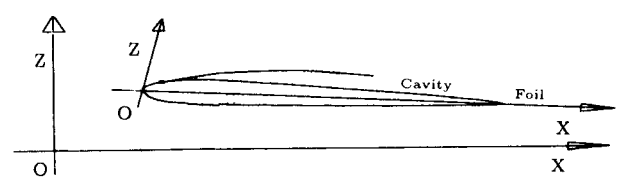

Figure 2. Coordinate system and schematic drawing of cavity model.

$\phi(p)$, on the body surface, S_B, a source distribution of strength, $\frac{\partial\phi(q)}{\partial n}$, on S_B and a normal dipole distribution of strength, $\triangle\phi$, on the wake surface S_W.

Discretization of Equation 18 leads to a linear system of algebraic equation for the unknown, ϕ:

$$2\pi\phi_i = \sum_{j=1}^{N_{tot}} C_{ij}(\phi_j) + \sum_{j=1}^{M} W_{ijl}(\triangle\phi)_j + \sum_{j=1}^{N_{tot}} S_{ij}\left(\frac{\partial\phi}{\partial n}\right)_j$$

$$i = 1, 2, \cdots, N_{tot}, \tag{19}$$

where C_{ij}, W_{ijl} (constant dipole distributions on body and wake surfaces) and S_{ij} (constant source distribution on body) are influence coefficients on panel j, acting on the control point of panel i. $(\frac{\partial\phi}{\partial n})_j$ is known from boundary condition (i) on the body surface but unknown on the cavity surface.

Iteration Scheme for the Cavity Surface

An open type model of sheet cavity is assumed, with a prescribed cavity length, located relative to the body at the first iteration. The open type model in the potential theory is a method to recover the pressure jump or stagnation point at the cavity trailing edge. However, it does imply that there is a pressure jump at the cavity trailing edge and, in fact, the pressure jump may exist, due to the collapsing of the bubble [7].

The next step is to calculate the cavity shape. From Equations 17 and 19, the potential on the body and source on the cavity surfaces may be determined.

The computed source strength, Q_c, (or normal derivative of the potential) on the cavity surface is not usually equal to the value prescribed in Equation 3 from KBC. Therefore, an iterative procedure is required to converge the $\triangle Q_c$, as described in Equation 20. The cavity thickness must be readjusted to make the flow on the cavity surface tangential to it.

$$\triangle Q_c = Q_c - \left.\frac{\partial\phi}{\partial n}\right|_{KBC} = Q_c + \vec{V}_I.\vec{n}. \tag{20}$$

The cavity thickness, t_c, can be calculated by integrating $\triangle Q_c/V_c$ over the cavity surface.

$$\frac{dt_c}{ds} = \frac{\triangle Q_c}{V_C}. \tag{21}$$

After integrating the above equation, the cavity thickness is obtained along the surface up to the specified gap at the cavity trailing edge.

$$t_c = \frac{1}{V_c}\int_0^{S_c} (Q_c + \vec{V}_I.\vec{n})ds. \tag{22}$$

At each iteration, the body and cavity surfaces are repaneled, based on the updated cavity surface, which was computed at the end of the previous iteration. In the next iteration, the new matrix element of Equations 17 and 19 are created, based on source and dipole singularities, then, the new potential on the body and the source on the cavity surfaces are determined. Again, from source strength, the new cavity thickness is obtained from Equation 22. This process is repeated to obtain the correct cavity shape. The present method and its iteration does not exceed 2-3 times and, in most cases, experience has shown that cavity shape is finally resolved during the first and second time of iteration.

Hydrodynamic Forces

The forces (F_X, F_Y, F_Z) acting on the hydrofoil can be calculated by integrating the pressure over the surface. They are expressed on the local coordinate system (x, y, z) as:

$$F_z = -\int_S (p - p_\infty) n_z ds,$$

$$F_y = 0,$$

$$F_x = -\int_S (p - p_\infty) n_x ds, \tag{23}$$

then, lift and drag on the hydrofoil are translated onto the fixed coordinate as follows,

$$L_h = F_z \cos\alpha - F_x \sin\alpha,$$

$$D_h = F_z \cos\alpha + F_x \sin\alpha, \tag{24}$$

where n_x and n_y are outward normal vectors on the hydrofoil or cavity surfaces.

The non-dimensional hydrodynamic coefficients of the hydrofoil are defined as follows:

$$\text{pressure coefficient:} \quad C_P = \frac{p - p_\infty}{1/2\rho V_0^2}, \tag{25}$$

$$\text{lift coefficient:} \quad C_L = \frac{L_h}{1/2\rho V_0^2 A}, \tag{26}$$

$$\text{drag coefficient:} \quad C_D = \frac{D_h}{1/2\rho V_0^2 A}. \tag{27}$$

The hydrodynamic characteristics of the propeller are obtained, as given below:

$$\text{advance ratio:} \quad J = \frac{V_A}{nD}, \tag{28}$$

$$\text{thrust coefficient:} \quad K_t = \frac{T}{\rho n^2 D^4}, \tag{29}$$

$$\text{torque coefficient:} \quad K_q = \frac{Q}{\rho n^2 D^5}. \tag{30}$$

All variables are described in the Nomenclature.

Calculation of Flow Field Velocity Around the Cavitating Body

From Green's theorem in the potential field, Equation 18, one can construct an alternative view of the problem in the velocity field. Taking the gradient of the perturbation velocity potential, the induced velocity can be expressed as:

$$4\pi\vec{v}(p) = \int_{S_B}\left\{\phi(q)\nabla_p\frac{\partial}{\partial n_q}\left(\frac{l}{R(p;q)}\right) - \frac{\partial\phi(q)}{\partial n_q}\nabla_p\left(\frac{l}{R(p;q)}\right)\right\}dS + \int_{S_W}\Delta\phi(q)\nabla_p\frac{\partial}{\partial n_q}\left(\frac{l}{R(p;q)}\right)dS. \quad (31)$$

Here, from the discretization of the body and wake and assuming that the potential and value of $\frac{\partial\phi(q)}{\partial n}$ are constant within each panel, then, Equation 31 can be written as follows:

$$\vec{v}(p) = \sum_{j=1}^{N_{tot}}(\phi_j)\nabla_p C_{ij} + \sum_{j=1}^{M}(\Delta\phi)_j\nabla_p W_{ijl} + \sum_{j=1}^{N_{tot}}\left(\frac{\partial\phi}{\partial n}\right)_j\nabla_p S_{ij}$$

$$i = 1, 2, \cdots, N_{tot}, \quad (32)$$

where $\nabla_p C_{ij}$, $\nabla_p W_{ijl}$ and $\nabla_p S_{ij}$ are the velocity influence coefficients.

Calculations of the velocity influence are more sensitive than the potential coefficient and, also, the required storage is three times more than the storage of the potential coefficient. One big advantage is that the velocities can be obtained directly for any of the field points.

NUMERICAL RESULTS AND DISCUSSIONS

In order to validate the present method, some experimental results from [8] have been selected for an elliptical hydrofoil of NACA0012, with aspect ratio = 3.0 and cavitation numbers σ = 0.91 and 1.30, at an angle of attack equal to 10°.

The elliptic hydrofoil were discretized by M = 15 panels in spanwise and $N + N_c$ = 35 panels in chordwise, therefore, the total panels became N_{tot} = 1050, as shown in Figure 3.

Also, a propeller model of SRI-123 was found in [9]. The propeller is 0.250 (m) in diameter and 6-bladed, with a 1.264 pitch ratio (at 0.7R). The

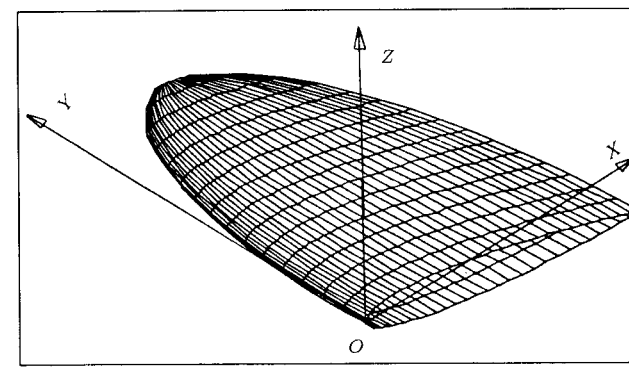

Figure 3. Paneling on elliptical hydrofoil NACA0012 (only half-span is shown).

Table 1. Main dimensions of the propellers.

Propeller Type	SRI-123
Diameter (m)	0.250
Exp. area ratio	0.80
Pitch ratio at 0.7R	1.264
Boss ratio	0.18
No. of blades	6
Rake angle (deg)	7.50
Skew angle (deg.)	12.5
Blade section	SRI-a

Table 2. Experimental cavitation test condition of propeller SRI-123.

J	V (m/s)	n (rps)	Cavitation Number, σ
0.5	2.5	20.0	0.43 0.58
0.7	3.5	20.0	0.30

main dimensions and cavitation test condition of the propeller are shown in Tables 1 and 2, respectively. The propeller is also discretized by M = 12 panels in radial and $N + N_c$ = 15 panels in chordwise. Thus, the total number of panels became 360 per blade and, plus hub, 60 per segment. Figure 4 shows the panel arrangement of the SRI-123 propeller.

Results For NACA0012 Hydrofoil

Cavity Shape

The computed result is compared with the experimental data of the cavity area, as shown in Figure 5, at two cavitation numbers for a 10° angle of attack. At σ = 1.30, the computed results show good agreement with experimental results but there is some discrepancy at cavitation number σ = 0.91, near the tip.

The results of cavity thickness at different spanwise locations (2Y/Span = 60%, 80%, 90%) for α = 10.0 deg and two cavitation numbers, 0.91 and 1.30, are shown in Figure 6. The computed thickness of the cavity is very thin near the tip, which gives the

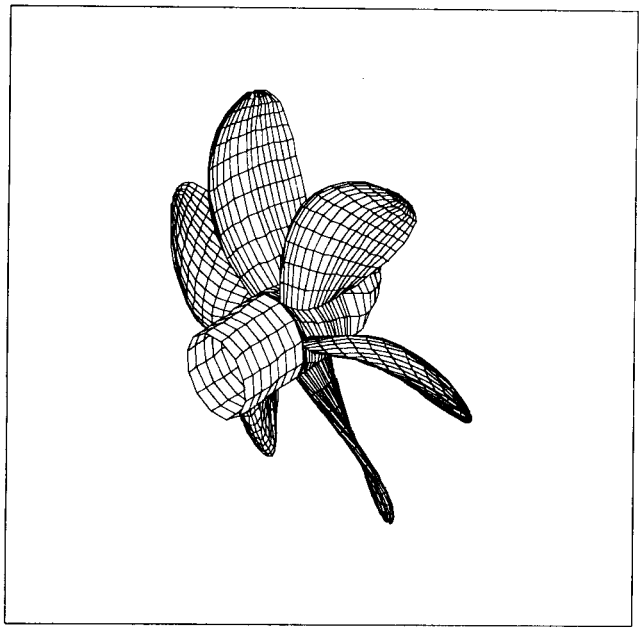

Figure 4. Panel arrangement of SRI-123 propeller.

lower cavity length. This may be one reason for the lower cavity length near the tip. The length of cavity grows with the decrease in cavitation number, as expected.

Pressure Distribution

As mentioned earlier, these calculations are based on sheet cavitation and do not include bubble cavitation, so the pressure is almost constant along the cavity surface and its value is equal to the cavitation number.

Comparison of the pressure coefficient distribution for Suction Side (SS) and Pressure Side (PS) on the hydrofoil surface (with and without cavitation) is shown in Figure 7, at different spanwise locations (2Y/Span = 60%, 80%, 90%), for $\alpha = 10°$ and for two cavitation numbers $\sigma = 1.30$ and $\sigma = 0.91$.

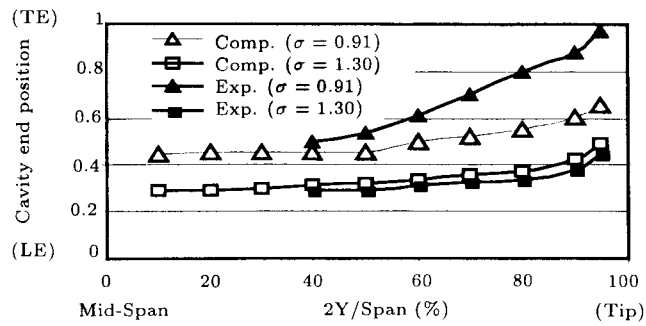

Figure 5. Comparison of cavity area on elliptical hydrofoil ($\alpha = 10.0°$).

Hydrodynamic Coefficients

It is very important to predict the hydrodynamic coefficients and the effect of cavity formation on them. The comparison of hydrodynamic coefficients of lift and drag are shown in Figure 8 for a non-cavitating and cavitating hydrofoil at an angle of attack equal to 10°. The computed lift and drag coefficients are close to the experimental results for a non-cavitating condition and the error is less than 3%.

The computed lift and drag are also shown in Figure 8 for a cavitating hydrofoil at a range of cavitation number between 0.5 and 1.3. Because the coefficients strongly depend on cavity length, where the pressure is constant and equal to the cavitation number, it is very important to have the correct cavity

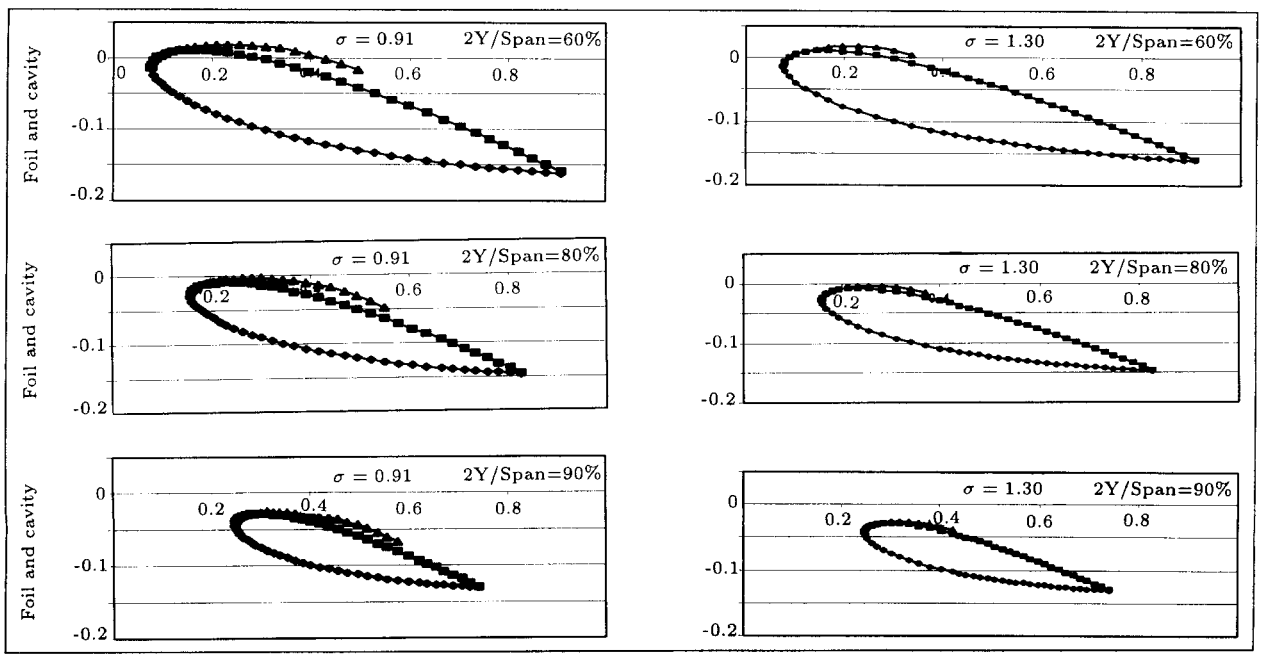

Figure 6. Cavity shape on elliptic hydrofoil with NACA0012 section (aspect ratio = 3.0 and $\alpha = 10.0°$).

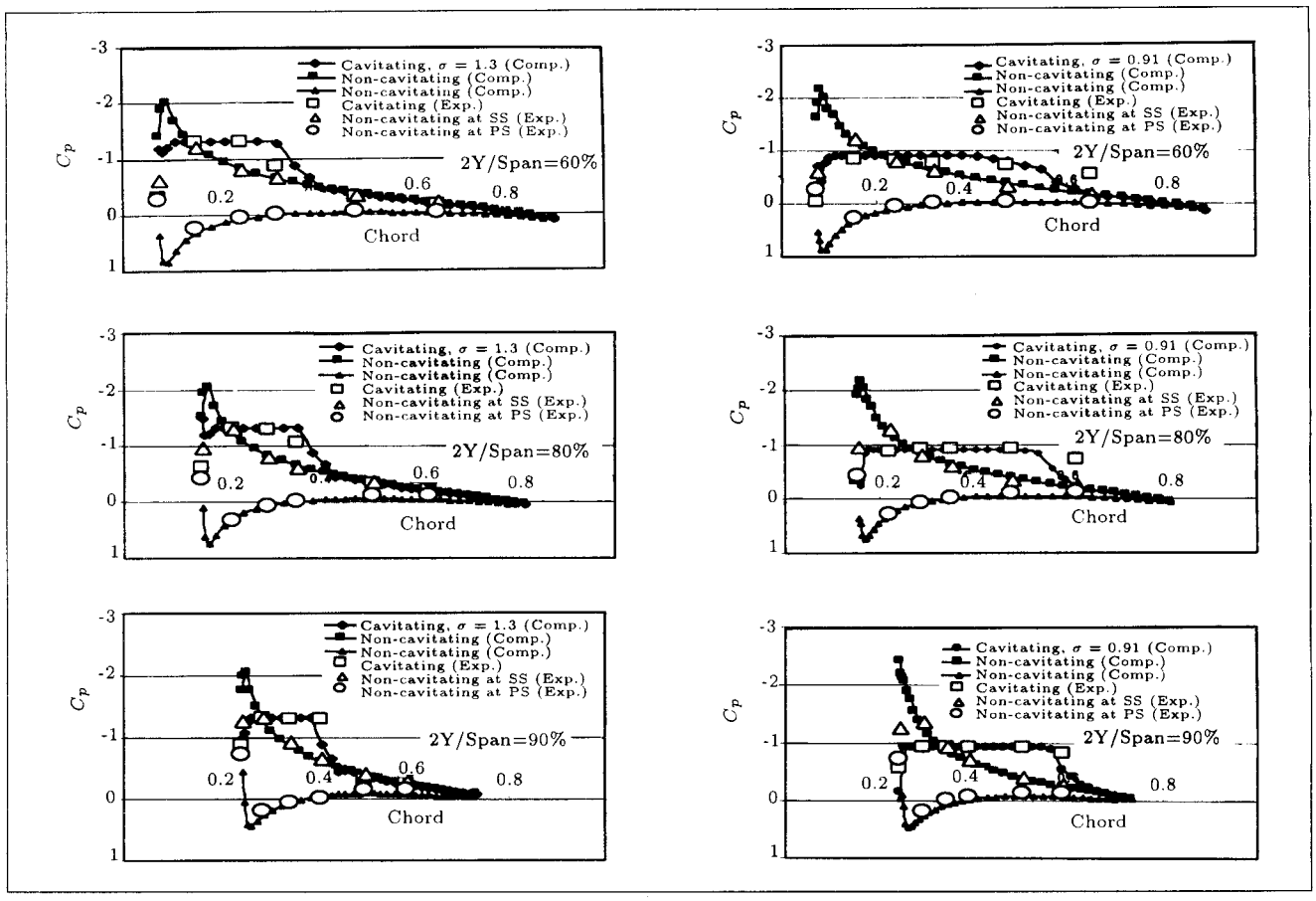

Figure 7. Comparison of pressure distribution on elliptic hydrofoil (NACA0012) with aspect ratio = 3.0 and $\alpha = 10.0°$.

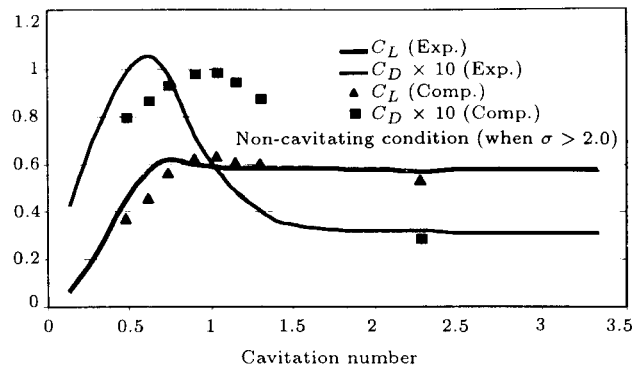

Figure 8. Comparison of lift and drag coefficient with variation of cavitation number for NACA0012 elliptic hydrofoil ($\alpha = 10.0$ deg).

length in order to give correct pressure distribution and hydrodynamic forces. The results in Figure 8 show the same trends as the experimental data but have slightly different values. The maximum value of the computed drag is 0.099 at a cavitation number equal to 1.0, but the experimental data shows 0.106 at a cavitation number equal to 0.62. The same deviation is obtained for lift, but less variance. The maximum lift coefficient was calculated to be 0.63, at a cavitation number of 1.0, but the experimental value is 0.62, at a cavitation number of 0.74.

Velocity Field Around the Cavitating Hydrofoil

Inspection of streamline patterns above the cavity region expose very clearly the fluid motion due to the volume of cavity. So, in the case of a ship propeller, it is important to obtain the cavity volume, which causes the fluctuation of the pressure on the ship's hull and the resulting vibrations. Figures 9 to 11 show different views of velocity vectors and theircorresponding isobars (axial velocity) in the flow field around the cavitating hydrofoils at different locations. Calculated induced velocities on the elliptical hydrofoil at 30% and 50% distance from the tip on NACA0012, with angle of attack $\alpha = 10.0°$ and cavitation numbers, 0.91 and 1.3, are shown in Figures 9 and 10.

Figure 11 shows the calculated induced velocities at the trailing edge and 50% from the leading edge, viewed from downstream, at the same condition on the elliptical hydrofoil. The cross flow at the tip is clearly shown in this figure. From the visualization of flow around the cavitating hydrofoil observed in [10,11], it seems that the present method can give good predictions of the flow field around the cavitating hydrofoil.

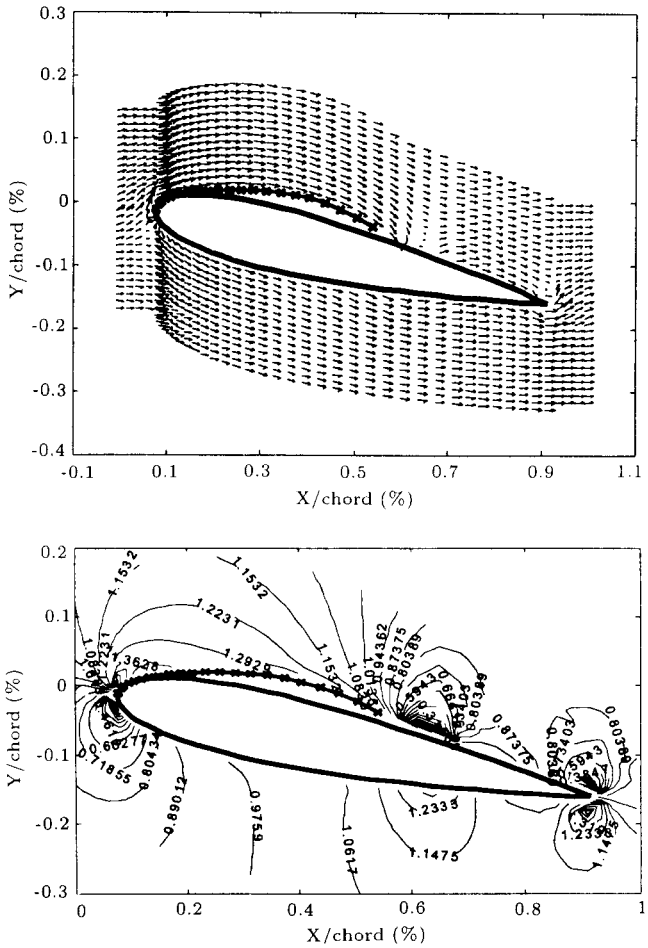

Figure 9. Calculated induced velocities on elliptical hydrofoil at 30% Distance from tip (NACA0012, $\alpha = 10.0°$, $\sigma = 0.91$).

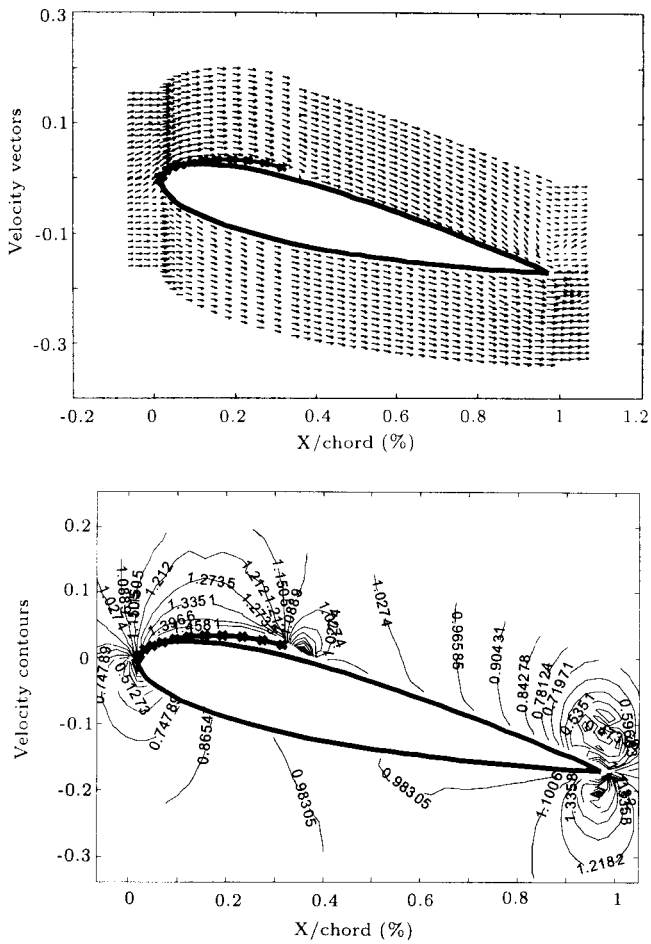

Figure 10. Calculated induced velocities on elliptical hydrofoil at 50% distance from tip (NACA0012, $\alpha = 10.0°$).

Results for SRI-123 Marine Propeller

The method is extended to predict the cavity shape and hydrodynamic characteristics of the propeller. Experimental data for propellers is scarce, especially pressure distribution. The SRI-123 marine propeller [9] was found to compare some available data.

Figure 12 shows the circulation distribution after imposing the pressure Kutta condition at advance coefficient, $J = 0.50$. Computations of pressure distributions on the SRI-123 propeller model are shown at $J = 0.5$ and 0.7 and at various radial locations ($r/R = 0.55, 0.7$ and 0.9) in Figure 13. It is also compared (at $r = 0.7$ R) with the available experimental data. It can be seen that the pressure distribution on the cavity surface is almost constant and equal to the cavitation number.

Comparisons of thrust and torque coefficients, K_t and K_q, are shown in Figure 14. They are compared with experimental data and a good agreement was found for the non-cavitating condition. The results for the cavitating condition at three different cavitation numbers, $\sigma = 0.30, 0.43$ and 0.58, are also shown in this figure. The effect of cavitation reduced the hydrodynamic coefficients, especially at low advance coefficient. Figure 15 shows alternative results of thrust and torque coefficients as a function of the cavitation number for the SRI-123 propeller at $J = 0.7$. It is concluded that when the cavitation number increases (at the same advance coefficient), the thrust and torque values converge and become constant, which means no cavitation will appear.

CONCLUSIONS

The present method is developed to predict the formation of a three-dimensional sheet cavity on a hydrofoil and a marine propeller. The approach is based on BEM, taking into account the hydrodynamic characteristics and flow field analysis. From the presented analysis, the following conclusions can be drawn:

- The method can evaluate accurately the hydrodynamic performance of the cavitating hydrofoil at different cavitation numbers and the results show good agreement with experimental results;

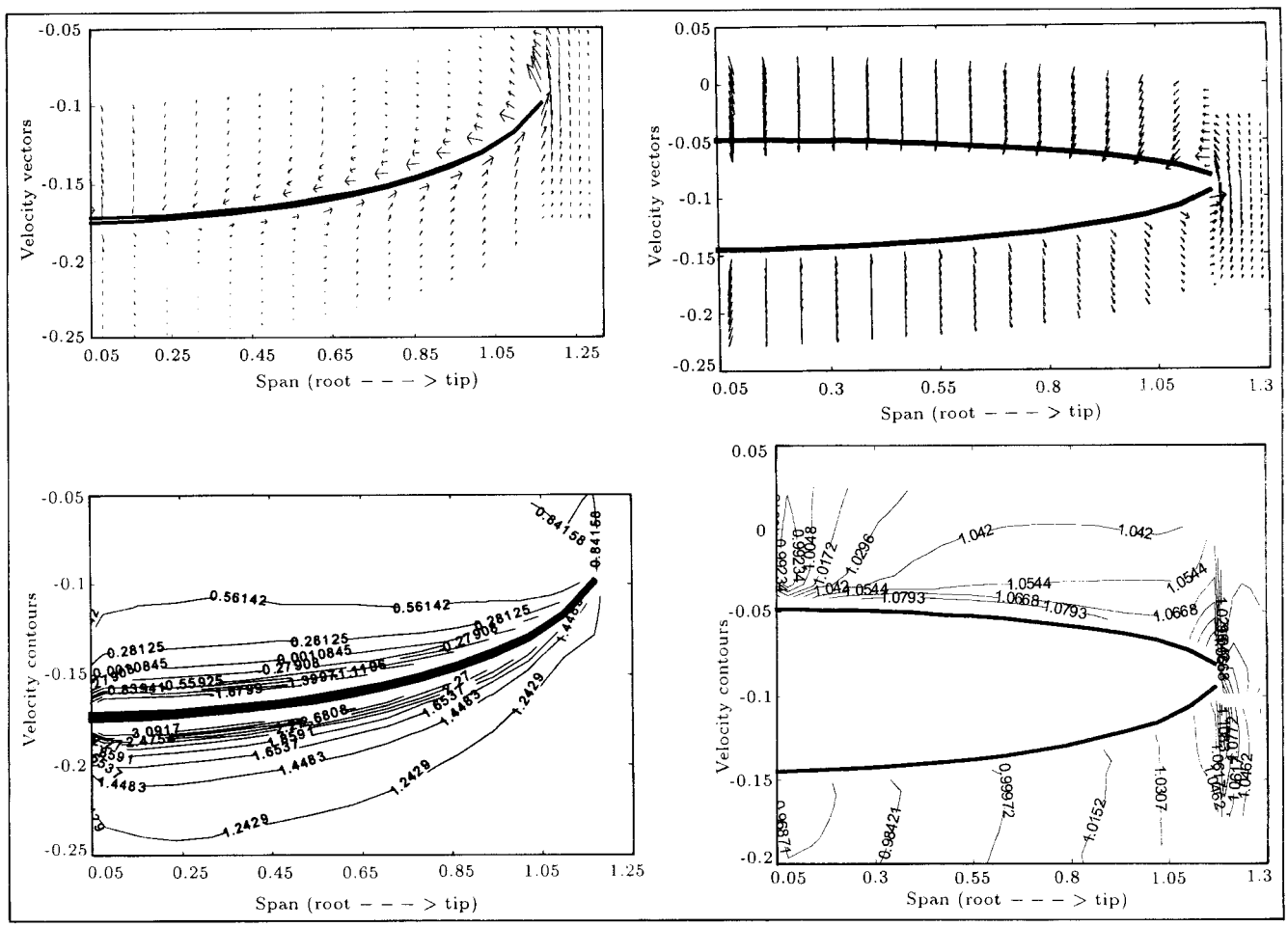

Figure 11. Calculated induced velocities at TE (two up) and 50% from LE (two down), view from downstream on elliptical hydrofoil NACA0012 ($\alpha = 10.0°$, $\sigma = 0.91$ (left) $\sigma = 1.30$ (right)).

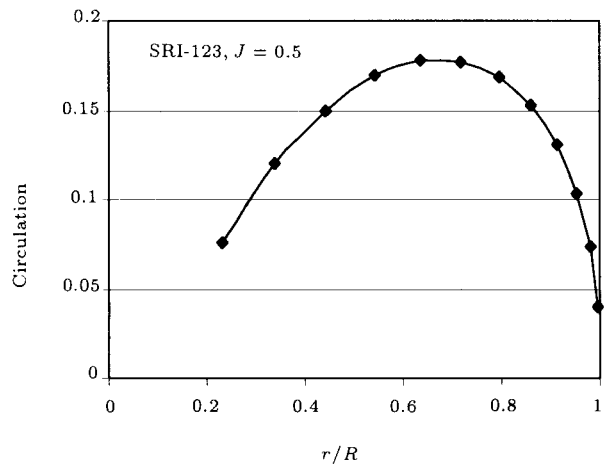

Figure 12. Circulation distribution on SRI-123 propeller model.

- This method successfully predicts the flow field around the cavitating hydrofoil, judged by comparison with data given in [10,11];
- It may be said that the method is able to find a good solution for the hydrodynamic characteristics of the marine propeller in a cavitating condition. Further investigation of the cavity separation point and cavity trailing edge and refinement of some boundary conditions should be developed, in order to achieve an exact cavity area, which is very important for hydrodynamic performance and cavitation prediction.

ACKNOWLEDGMENT

The author would like to thank the NSERC (Natural Sciences and Engineering Research Council) of Canada for a grant-in-aid of this research. He also greatfully acknowledg the useful discussions, comments and help, along with the relevant references of Prof. Neil Bose of the Memorial University of Newfoundland, Canada, and Prof. Kuniharu Nakatake of the Kyushu University, Japan.

NOMENCLATURE

A	area of hydrofoil

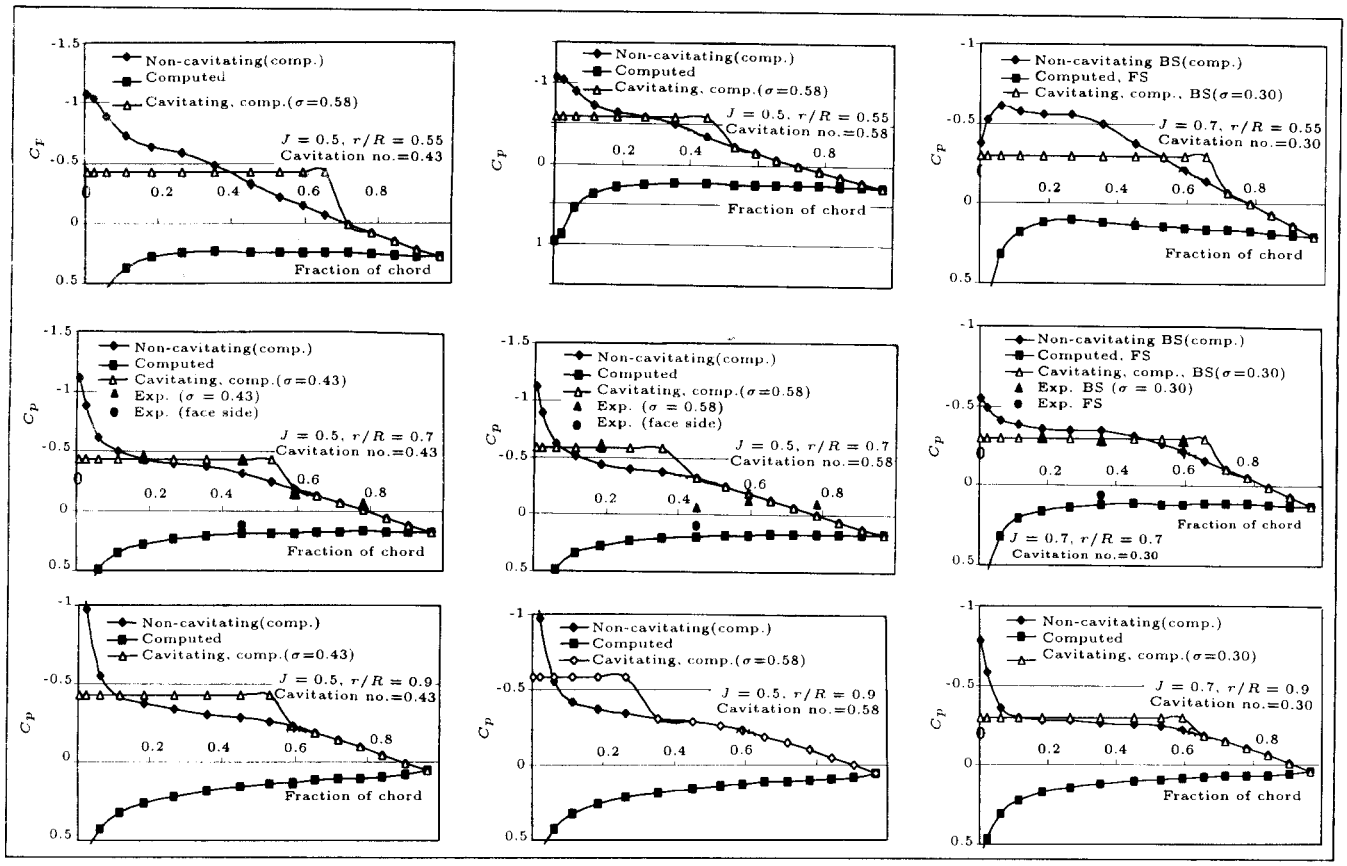

Figure 13. Pressure distribution on SRI-123 cavitating propeller model.

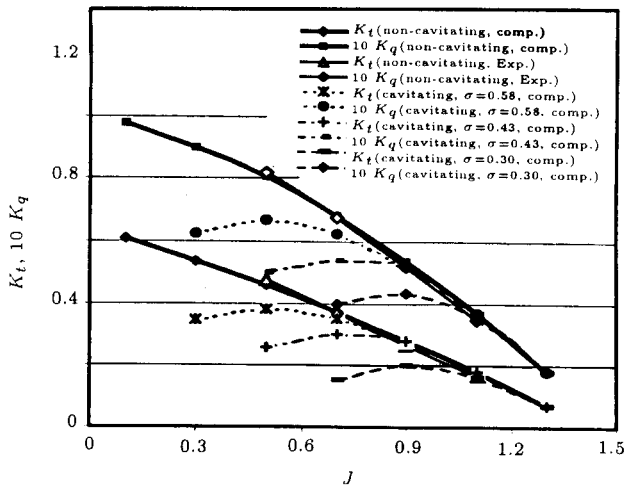

Figure 14. Open water characteristics of SRI-123 propeller model at cavitating and non-cavitating conditions.

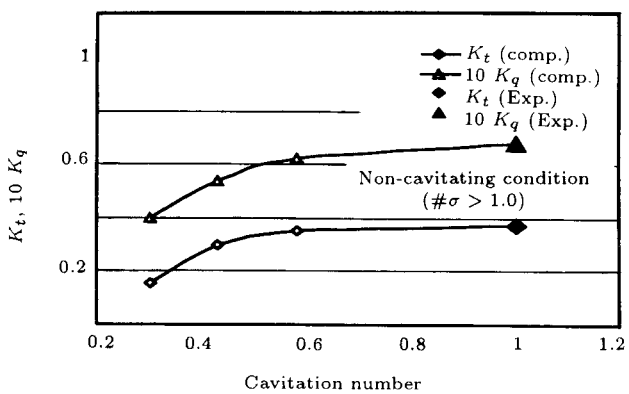

Figure 15. Thrust and torque coefficients with variation of cavitation number for SRI-123 propeller at $J = 0.7$.

C_p	pressure coefficient
C_L	lift coefficient
C_D	drag coefficient
D	propeller diameter
D_h	drag on hydrofoil
F_X, F_Y, F_Z	forces on hydrofoil
L_h	lift on hydrofoil panels
l_d	cavity starting point
K_t	thrust coefficient
K_q	torque coefficient
J	advance coefficient
M	number of spanwise panels
N	number of chordwise panels (on non-cavity)
N_c	number of chordwise panels (on cavity)

N_{tot}	number of total panels
$N + N_c$	total number of chordwise panels
n	rotating speed of propeller
$\vec{n}$	outward normal unit vector
p	pressure on the body surface
p_∞	static pressure
p_c	cavity (vapor) pressure
Q	propeller torque
Q_c	strength of source on cavity
s, ν	non-orthogonal abscissa
S_B	body surface
S_C	cavity surface
S_W	wake surface
T	propeller thrust
t_c	cavity thickness
$\vec{x}$	position vector on body
$\vec{x}_c$	position vector on cavity
U, L	upper and lower sides indexes
V_A	advance speed
$\vec{V}_I$	local inflow velocity
$\vec{V}_S$	chordwise velocity
$\vec{V}_c$	tangential velocity on cavity surface
$\vec{V}_r$	cross-flow velocity
$\vec{V}_T$	interacted tangential velocity
$\vec{\nu}(p)$	induced velocity at any field point
$\partial\Phi/\partial s$	chordwise derivative of potential
$\partial\Phi/\partial\nu$	spanwise derivative of potential
$\partial\phi/\partial n$	normal derivative of potential
ϕ_I	inflow velocity potential
ϕ	perturbation velocity potential
Φ	total velocity potential
$\triangle\phi$	strength of dipole on wake
σ	cavitation number
ρ	mass density of fluid
α	hydrofoil angle of attack
Γ	non-dimensional circulation at TE
C_{ij}, W_{ijl}	dipole influence coefficients
S_{ij}	source influence coefficient
$\nabla C_{ij}, \nabla W_{ijl}$	gradient dipole influence coefficients
∇S_{ij}	gradient source influence coefficient

REFERENCES

1. Lee, C.S. "Prediction of the transition cavitation on marine propeller by numerical lifting surface method", *Proceeding of the 13th Symposium on Naval Hydrodynamics*, Tokyo (1980).
2. Kinnas, S.A. and Fine, N.F. "A numerical nonlinear analysis of the flow around two- and three-dimensional partially cavitating hydrofoils", *J. of Fluid Mechanics*, **245**, pp 151-181 (1993).
3. Fine, N.E. and Kinnas, S.A. "A boundary element method for the analysis of the flow around 3-D cavitating hydrofoils", *J. of Ship Research*, **37**(3), pp 213-224 (1993).
4. Ando, J., Matsumoto, D., Maita, S., Ohashi, K. and Nakatake, K. "Calculation of three-dimensional steady cavitation by a simple surface panel method", *J. of Society of Naval Architects of Japan*, **186**, pp 17-27 (in Japanese) (1999).
5. Ghassemi, H. "A study on hydrodynamic analysis of propellers and cavitation prediction of hydrofoils by the application of surface panel method", Ph.D. Dissertation, Yokohama National University, Yokohama, Japan (1997).
6. Kubota, A., Kato, H. and Yamaguchi, H. "A new modeling of cavitating flows: A numerical study of unsteady cavitation section", *J. of Fluid Mechanics*, **240**, pp 59-96 (1992).
7. Ohkusu, M., *Advances in Marine Hydrodynamics*, Chapter 5, Cavitation, Computational Mechanics Publications, pp 233-278 (1996).
8. Takasugi, N., Yamaguchi, H., Kato, H. and Maeda, M. "An experiment of cavitating flow around a finite span hydrofoil", *Society of Naval Architects of Japan*, **172**, pp 257-265 (in Japanese) (1992).
9. Kadoi, H., Kokubo, Y., Koyama, K. and Okamoto, M. "Systematic tests on the SRI-a propeller", *Report of Ship Research Institute of Japan*, **15**(2), pp 43-68 (in Japanese) (1978).
10. Kato, H., Yamaguchi, H., Shigemitsu, H., Harada, M. and Takasugi, N. "Study on flow and cavitation around a finite span swept-back hydrofoil", *Society of Naval Architects of Japan*, **176**, pp 43-50 (in Japanese) (1995).
11. Laberteaux, K. and Ceccio, S. "Partial attached cavitation on two and three-dimensional hydrofoils", *22nd Symposium on Naval Hydrodynamics* (1998).